# Godunov Computational Fluid Dynamics Method for Extreme Flow Velocities and Any Equation of State

D. W. Bogdanoff* and D. C. Brackett†
*University of Washington, Seattle, Washington*

**An inviscid computational fluid dynamics code that can handle multiple component species, simple chemical reactions, a completely general equation of state, and velocities up to hundreds of kilometers per second is described. Radiation effects are not included. The code uses a sliding grid technique to handle multiple moving zones containing different media. Third-order extrapolations and interpolations are used to determine cell boundary values of the primitive variables. Limiting techniques then are applied to these values to maintain code accuracy and stability. First- and second-order Godunov procedures are used to calculate the cell boundary fluxes. The cell center values are updated in time using an explicit MacCormack predictor-corrector technique that is second-order accurate in time. The code was proofed with benchmark test cases, including Riemann's shock tube problem at pressure ratios up to $10^4$, impacts of ideal-gas and dense media zones at closing velocities up to 220 km/s, detonation waves in stoichiometric hydrogen-oxygen mixtures, ideal-gas wedge and cone flows, and a wedge flow of iron at a speed of 110 km/s. The results of these proof tests are discussed. The agreement between the CFD results and the exact solutions is found to be excellent.**

## I. Introduction

In our research group, experimental and theoretical investigations are being carried out on the acceleration of projectiles using chemical ramjet-in-tube concepts. Using combustible gases,[1-3] high explosives,[4] and high explosives plus linear velocity multiplication techniques,[4,5] it may be possible to achieve velocities of 8–12, 20–30, and 50–100 + km/s, respectively. For our theoretical studies, it was necessary to construct computational fluid dynamics (CFD) codes with severe capability requirements not met by most codes in the literature. Our new CFD code had to be able to handle 1) multiple chemical species, 2) simply modeled chemical reactions, 3) a completely general equation of state, 4) velocities up to hundreds of kilometers per second, 5) multiple zones with sliding boundaries to preserve media integrity, and 6) higher-order calculations in space to limit numerical dissipation.

Many of possible candidate codes appearing in the literature use a form of "flux splitting" that requires the Euler equations to be homogeneous of degree one. This requires that the media have an equation of state (EOS) of the form $p = \rho f(e)$, where $p$ denotes the pressure, $\rho$ the density, and $e$ the internal energy.[6,7] Also, the matrices used to diagonalize the flux-state variable Jacobian usually are given in a form suitable only for use with an ideal-gas EOS.[6] These matrices can be obtained in a more general form,[8] but the basic assumption in this technique that the Euler equations are homogeneous of degree one still will produce large errors if used, for example, with a dense media EOS. The errors can be reduced if the flux-splitting procedure is applied as a correction[9] to a flux calculated directly from the state variables. However, large errors still can occur with this latter procedure at sufficiently large velocities or pressure ratios. The Godunov flux calculation procedure,[10,11] which solves a one-dimensional Riemann problem at the boundaries between cells, has an advantage that no restrictions on the form of the EOS are required. The results presented in this paper were obtained using a Godunov procedure with higher-order spatial differencing. The Godunov flux calculation procedure itself may be extended to second order.[11] With the Godunov flux calculation technique and careful attention to extrapolation, interpolation and limiting techniques, good solutions were obtained for completely general equations of state at velocities up to hundreds of kilometers per second.

Presented in part as Paper 87-1978 at the AIAA/SAE/ASME/ASEE 23rd Joint Propulsion Conference, San Diego, CA, June 29–July 2, 1987; received Jan. 15, 1988; revision received Aug. 8, 1988. 

*Research Engineer, Aerospace and Energetics Research Program; currently Senior Research Scientist, Aerothermodynamics Branch, NASA Ames Research Center, Moffett Field, CA. Member AIAA.

†Graduate Student, Aerospace and Energetics Research Program; currently Senior Engineer, Electronics Systems Technology, Boeing Aerospace, Kent, WA. Student Member AIAA.

## II. Numerical Procedures

### A. Multiple Zoning

Both one- and two-dimensional codes (planar and axisymmetric) have been constructed. The codes can be divided in the $y$ or radial direction into multiple zones containing different media. The grids can slide in the $y$ direction to preserve the integrity of the media of the zones.

### B. Governing Equations

The two-dimensional Euler equations, written in conservation form, are

$$\frac{\partial U}{\partial t} + \frac{\partial F}{\partial x} + \frac{\partial G}{\partial y} = 0 \tag{1}$$

where the state vector $U$ is given by

$$U = (\rho, \rho u, \rho v, e_t, \rho m_1, \rho m_2, \ldots) \tag{2}$$

and the flux vectors $F$ and $G$ in the $x$ and $y$ directions are given by

$$F = (\rho u, \rho u^2 + p, \rho uv, u(e_t + p), \rho u m_1, \rho u m_2, \ldots) \tag{3a}$$

$$G = (\rho v, \rho vu, \rho v^2 + p, v(e_t + p), \rho v m_1, \rho v m_2, \ldots) \tag{3b}$$

where $e_t$ denotes the total energy per unit volume, $u$ the axial velocity, $v$ the radial or $y$ direction velocity, $m_i$ the mass fraction of the $i$th component, and $e_t = \rho(e + u^2/2 + v^2/2)$. The speed of sound $c$, temperature, and $p$ are obtained from

$\rho$ and $e$ using the EOS. The code uses the finite-volume technique. The state variables are calculated at the center of each computational cell.

### C. Determination of Cell Boundary Values

The fluxes at the cell boundaries are calculated from values of the primitive variables ($\rho$, $u$, $v$, $e$, $m_i$) on the two sides of the boundary. The cell boundary values are obtained by extrapolation and/or interpolation from the cell center values. Most of the calculations of internal cell boundary values are done with third-order extrapolations/interpolations. The extrapolations/interpolations are not always simple parabolic fits, however. If the three points being curve fitted are so disposed to imply nonmonotonic behavior over their range, the third-order curve fits are replaced by lower-order fits. A smoothly blended transition is made between the third-order fits (used when the three points are well behaved) and the lower-order fits. The final third-order boundary value at each side of a cell boundary is taken to be $\zeta \times$ (extrapolated value) + $(1 - \zeta) \times$ (interpolated value), where $\zeta$ is a constant. Generally, for internal cell boundaries, third-order procedures with $\zeta \simeq 0.5$ give the best results. Further details are given in Appendix A.

The limiting procedures will be described with reference to Fig. 1. In the figure, the abscissa is the extrapolated/interpolated value before limiting; the ordinate is the corresponding value after limiting. Values at the cell centers bracketing the cell boundaries in question are $x_{ba1}$ and $x_{ba2}$. The extrapolation/interpolation is performed from the side of the boundary corresponding to the cell center value $x_{ba1}$. An essential limiting procedure which must be applied is that no extrapolated/interpolated value can lie outside the range of the two adjoining cell center values. The simplest way of replacing such unacceptable extrapolated/interpolated values is by the cell center value from the extrapolation/interpolation side (i.e., line 1 in Fig. 1). This technique is very stable but is unnecessarily diffusive. The numerical diffusion can be reduced by, instead, replacing the unacceptable extrapolated/interpolated value with whichever of the two cell center values is closest to the unacceptable value (i.e., line 2 in Fig. 1). This procedure, while greatly reducing diffusion, tends to reintroduce some solution oscillation problems. The best compromise procedure we have found to date is as follows. If the extrapolated/interpolated value is beyond the cell center value on the extrapolation/interpolation side (the "near" side) of the boundary, that cell center value is used instead. We will refer to the opposite side of the boundary as the "far" side. A certain value for the primitive variable is chosen, that is $\eta = \xi \times$ (far-side value) + $(1 - \xi) \times$ (near-side value), where $\xi$ is a constant. When the extrapolation/interpolation value is beyond $\eta$ in the direction of the far side, it is replaced by $\eta$. This procedure is shown as line 3 in Fig. 1. Our best results have been obtained with $\xi \simeq 0.5$.

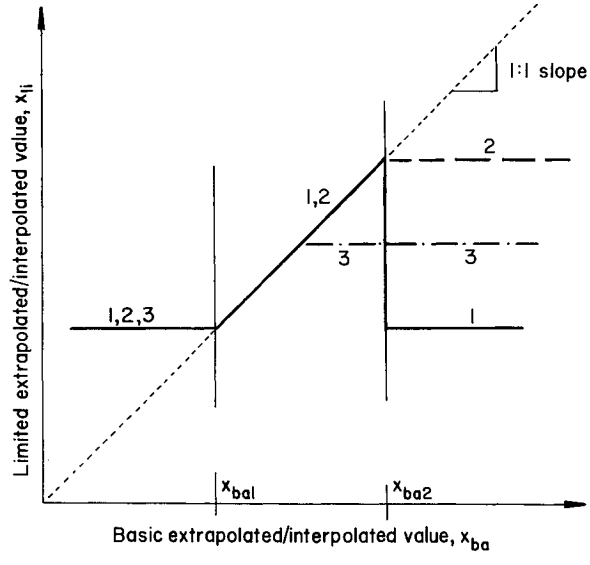


**Fig. 1 Illustration of limiting procedures. The abscissa is the extrapolated/interpolated value before limiting, the ordinate the corresponding value after limiting, $x_{ba1}$ and $x_{ba2}$ the values at the cell centers bracketing the cell boundary in question. Lines 1-3 represent the three cases discussed in the text.**

To avoid wiggles in the neighborhood of strong wave systems in very-high-velocity flows (above ~ 30 km/s), in addition to the preceding limiting procedure, we have usually found it necessary to apply the following "strong wave limiting" (SWL) technique. We believe that the necessity for this procedure is as follows. In the region of very strong waves, some primitive variables, such as internal energy and pressure, can change by many orders of magnitude over the space of a few cells. The structure of our extrapolation/interpolation and limiting procedures discussed above is insufficient to control the accuracy of the extrapolated/interpolated primitive variables in some of these cases. What has been added is to test the extrapolation/interpolation range for the presence of very strong waves and, if they are found, to revert from third-order to first-order procedures. To make these tests, differences in normalized velocities, pressures, and acoustic impedances are examined over the extrapolation/interpolation range. The following paragraph presents more details.

In the direction normal to the cell boundary in question, the following quantities are calculated between all adjacent pairs of cells within the extrapolation/interpolation range:

$$\beta_{1i} = \frac{|u_{i,\perp} - u_{i+1,\perp}|}{\min(c_i, c_{i+1})} \tag{4}$$

$$\beta_{2i} = \frac{|p_i - p_{i+1}|}{\min(\rho_i c_i^2, \rho_{i+1} c_{i+1}^2)} \tag{5}$$

$$\beta_{3i} = \frac{|\rho_i c_i - \rho_{i+1} c_{i+1}|}{\min(\rho_i c_i, \rho_{i+1} c_{i+1})} \tag{6}$$

The subscripts $i$ and $i + 1$ denote any two adjacent cells within this range; $u_{i,\perp}$ and $u_{i+1,\perp}$ denote velocities normal to the boundary. Equation (4) compares normal velocity differences with speeds of sound, Eq. (5), pressure differences with the elastic modulus of the media $\rho c^2$, and Eq. (6), differences in the acoustic impedance $\rho c$ wih the acoustic impedances themselves. For any cell boundary, all three $\beta$ values are examined over the relevant range. The maximum $\beta$ value, $\beta_m$, is found. First- or higher-order extrapolations/interpolations or a blend are used according to the value of $\beta_m$ (see Table 1); $\alpha_1$ and $\alpha_2$ are critical values and $\zeta = (\beta_m - \alpha_2)/(\alpha_1 - \alpha_2)$. Abrupt switching between first and higher order produced poor results so a smooth blend was used for $\alpha_1 > \beta_m > \alpha_2$ (Table 1). Most of our results at velocities above ~ 30 km/s were obtained using SWL techniques with $\alpha_1$ between 1.4 and 4.0 and $\alpha_2$ between 0.7 and 2.0. The SWL technique is not used in most of the flowfield but only in the neighborhood of very strong wave systems.

### D. Flux Calculation Procedure

The first-order Godunov procedure is briefly described here. All Godunov procedures are done in rotated coordinate systems so that the new (rotated) $x$ and $y$ coordinates are normal and parallel to the cell boundary, respectively. A vertical cell boundary with state 1 to the left and state 5 to the right is considered. In general, solution of the one-dimensional Riemann problem will produce two new zones, 2 and 4 (the ordering of the zones is 1-5, left to right), two waves (12 and 45), propagating to the left and right relative to the media, respectively, and a contact surface 24 dividing zones 2 and 4. Applying the characteristic equations

$$dp = -\rho c\, du \tag{7}$$

$$dp = \rho c\, du \tag{8}$$

**Table 1 Selection of first- or higher-order extrapolation/interpolations depending on $\beta_m$**

| $\beta_m$ range | Extrapolation/interpolation technique |
|---|---|
| $\beta_m > \alpha_1$ | First order |
| $\alpha_1 > \beta_m > \alpha_2$ | $\xi \times$ (first order) + $(1 - \xi) \times$ (higher order) |
| $\alpha_2 > \beta_m$ | Higher order |

**Table 2 Selection of first- or higher-order Godunov calculations depending on $\beta_{mg}$**

| $\beta_{mg}$ range | Godunov calculation technique |
|---|---|
| $\beta_{mg} > \alpha_{1g}$ | Second order |
| $\alpha_{1g} > \beta_{mg} \alpha_{2g}$ | $\xi_g \times$ (second order) + $(1 - \xi_g) \times$ (first order) |
| $\alpha_{2g} > \beta_{mg}$ | First order |

across waves 12 and 45 allows $p_2 = p_4$ and $u_2 = u_4$ to be determined. Using the $u$ characteristic equations

$$de = \frac{p\, d\rho}{\rho^2} \tag{9}$$

and the EOS between states 1 and 2 and 4 and 5 allows $\rho_2$, $\rho_4$, $e_2$, and $e_4$ to be determined. From the velocities of the waves 12 and 45 and the contact surface 24, the zone in which the cell boundary will reside during the current time step can be determined and the fluxes determined from the primitive variables in that zone. Transverse velocities and mass fractions are assumed to remain unchanged across the waves and to change only at the contact surface.

It is necessary to limit the Godunov predictions of $p$, $\rho$, and $e$ to positive values or, for $p$, to the spall strength of the media. Under severe expansion conditions, it may be necessary to include a void zone 3 between zones 2 and 4. The calculation of wave velocities requires care. Let 45 be an expansion wave. The wave velocity then can safely be taken to be $[(u_4 + c_4) + (u_5 + c_5)]/2$. If 45 is a compression wave, this value cannot always be used, since it may become smaller than the contact surface velocity $u_4$, producing an inconsistent solution. A satisfactory first-order wave velocity in this case is $u_4 + c_5$. The same care must be taken with the velocity of wave 12.

At extremely high velocities, it is necessary to have higher-order-accuracy Godunov procedures (or "Riemann solvers") available to maintain the overall solution accuracy. Roe has developed a Riemann solver that returns exact solutions when the two state points lie on opposite sides of a shock wave or a contact discontinuity. (Roe's work is well described in Ref. 12.) This is true, however, only when the medium has perfect-gas EOS. Reference 11 presents a second-order Riemann solver that uses a particular pressure-velocity relation for compression (shock) waves; for expansion waves, this same compression wave relation is translated and inverted. Our second-order Godunov procedure uses the same pressure-velocity relation for compression waves as does Ref. 11. (Our procedure, however, was derived before we were aware of Ref. 11.) For expansion waves, we use two-term Taylor series expansions about the initial state point, which should be more accurate than the procedure of Ref. 11.

In our second-order Godunov procedure, Eqs. (7) and (8) are replaced with the appropriate quadratic relations between $p_2$ $(= p_4)$ and $u_2$ $(= u_4)$, which can be solved for $p_2$ and $u_2$. Second-order-accurate integrations of Eqs. (7–9) are used to obtain $\rho_2$, $\rho_4$, $e_2$, and $e_4$. Different integrations are used for expansion and compression waves; for the latter, shock wave relationships are used extensively. No iterative procedures are required. Further details are presented in Appendix B.

The decision of whether to use first- or second-order Godunov procedures at a given cell boundary is handled as follows: $l$ and $r$ denote conditions on the two sides of the cell boundary in question. We calculate

$$\beta_{1g} = \frac{|u_{l\perp} - u_{r\perp}|}{\min(c_l, c_r)} \tag{10}$$

$$\beta_{2g} = \frac{|p_l - p_r|}{\min(\rho_l c_l^2, \rho_r c_r^2)} \tag{11}$$

where $\beta_{1g}$ and $\beta_{2g}$ give two measures of the strength of the waves that will be produced at the cell boundary on the solution of the Riemann problem; $\beta_{mg}$ is the greater of $\beta_{1g}$ and $\beta_{2g}$. We choose two critical values $\alpha_{1g}$ and $\alpha_{2g}$. The fluxes are calculated according to the relative values of $\beta_{mg}$, $\alpha_{1g}$, and $\alpha_{2g}$ as shown in Table 2. $\zeta_g$ is equal to $(\beta_{mg} - \alpha_{2g})/(\alpha_{1g} - \alpha_{2g})$. Most of our results have been obtained with $\alpha_{1g} = 0.7$ and $\alpha_{2g} = 1.4$. These values are such that the second-order Godunov technique is used only at a few cell boundaries, in the neighborhood of strong wave systems. This is desirable, since the second-order Godunov procedure is more expensive computationally than the first-order one. The smooth blending between first- and second-order Godunov procedures was necessary to obtain the best quality solutions. An abrupt switch between these two procedures had a tendency to produce oscillations in the solutions. No added smoothing or damping was used in the codes, other than that inherent in the extrapolation/interpolation, limiting, and flux calculation procedures.

We recapitulate the flux calculation procedure briefly. Using the extrapolation, interpolation, and limiting procedures described earlier, the primitive variables on the two sides of the cell boundary in question are obtained. Then, a one-dimensional Riemann problem is solved to first- or second-order accuracy to yield, usually, two waves, a contact surface, and four media zones. The zone in which the cell boundary will reside during the current time step is determined, and the fluxes are calculated from the primitive variables in that zone. Transverse velocities and mass fractions are assumed to remain unchanged across the waves and to change only at the contact surface.

### E. Equations of State

The EOS options currently available in the codes are 1) perfect gas, both volumetrically and calorically; 2) perfect gas volumetrically with $e = \int C_v\, dT$ taken from the JANAF tables[13]; 3) Zel'dovich and Raizer's three-term EOS[14,15] with the third term neglected; 4) an EOS for gases of the form $p(v - b) = RT$, where the "molecular volume" is taken to be compressible in accord with Zel'dovich and Raizer's cold compression $p - v$ expression[15]; and 5) the tabular SESAME EOS data[16] from the Los Alamos Scientific Laboratory. In the above, $C_v$ denotes specific heat at constant volume, $T$ the temperature, $v$ the volume, $b$ the molecular volume, and $R$ the gas constant of the gas.

### F. Boundary Conditions

Consider a one- or two-dimensional solution geometry that is multizoned in the up-and-down ($y$ or radial) direction. For two-dimensional geometries, the flow enters on the left side and leaves on the right side. One of the following boundary conditions is imposed at each zone boundary (excluding the in- and outflow boundaries): 1) normal velocity specified (e.g., zero normal velocity at a stationary boundary); 2) pressure specified (e.g., zero pressure at a free surface); or 3) normal velocity and pressure matched across the zone boundary (e.g., at a media interface).

To obtain values for the primitive variables at the zone boundaries (to be used as input in Godunov procedures), extrapolations and limiting procedures are used that are very similar to those used for the cell boundary calculations. There are some differences, however, because of the unavailability of certain cell center data on the far side of the zone boundary.

With the primitive variables extrapolated to the zone boundary, first- and second-order Godunov procedures are used to find whichever (or both) of the variables, pressure and normal velocity, is required at the zone boundary.

For internal cell boundaries one cell removed from zone boundaries, excluding left- and right-side inflow and outflow zone boundaries, two additional "virtual" cells are created by "reflecting" the two cells nearest the zone boundary about the boundary. Using these virtual cells, extrapolations/interpolations in both directions can be made to obtain the primitive variables on the two sides of the cell boundary in question and then the fluxes. Third-order extrapolations/interpolations involving the reflected cells were found to produce erratic results, so second-order extrapolations/interpolations were used instead. It is recognized that this reflection procedure is equivalent to assuming that the flow is locally one-dimensional and that the zone boundary in question moves at a constant velocity. Using this reflection procedure therefore could produce difficulties under certain circumstances, e.g., strong curvature of the zone boundary. Under such conditions, more sophisticated procedures may be required. However, we have not found any difficulties attributable to our reflection procedure to date.

For two-dimensional calculations, at the left side where the flow enters, the flow is supersonic and the boundary conditions are held at prescribed values. At the right side where the flow exits, the boundary condition values are set equal to those one cell upstream of the boundary. This is correct for supersonic exiting flow and is equivalent to nonreflecting boundary conditions[17] for subsonic exiting flow.

### G. Advancement of Code in Time

The code employs an explicit MacCormack predictor-corrector differencing scheme[18] that is second-order accurate in time. The solution to Eq. (1) is advanced in time for the predictor and corrector steps as follows (including only the $F$ flux for simplicity):

$$\overline{U^{n+1}V^{n+1}} = U^nV^n + \sum F_pA\,\Delta t \tag{12}$$

$$U^{n+1}V^{n+1} = \tfrac{1}{2}(U^nV^n + \overline{U^{n+1}V^{n+1}} + \sum F_cA\,\Delta t) \tag{13}$$

where $U$ is the state vector, $V$ the cell volume, $A$ the cell wall area, $F_p$ and $F_c$ the fluxes, $\Delta t$ the time step, and $n$, $n+1$, and $n+1$ the conditions at the beginning of the time step and at the end of the predictor and corrector time steps, respectively. When the computational grid slides, $V^n \neq \overline{V^{n+1}} \neq V^{n+1}$ and the areas must be carefully averaged values. Otherwise, spurious source terms can be generated. If cell center $e$ or $\rho$ values calculated from Eqs. (12) and (13) are less than zero, they are reset to a fraction, typically 0.2, times the value at the beginning of the time step. This safety device is invoked only very rarely, when very strong shock waves are present. Since the method is explicit, the von Neumann stability criterion[19] that the CFL number be less than 1 must be applied. Most of our results were obtained with a CFL number of 0.6.

### H. Combustion Modeling

Gas combustion is modeled with a single global Arrhenius expression for reactants→products. The products include all major mass fraction species with fixed mass fractions determined from separate equilibrium combustion calculations. The Arrhenius constants were determined for the hydrogen-oxygen combustion results presented here by adjusting them to fit the experimental data of Ref. 20. To avoid nonphysical propagation of detonation waves against a strong convection velocity across the grid structure, it is necessary to permit the consumption of 15%, at most, of the reactant mass originally present in a cell, per time step. Each computation time step consists of a Euler solver step with frozen chemistry, followed by a chemical reaction step in isolated cells without flow interaction. Both steps are second-order accurate in time.

### I. Convergence: Code Acceleration Techniques

When steady-state solutions are sought, the convergence of the solution is judged using a density residue. This residue is a root mean square average, over all the computational cells, of the fractional density change per time step. In typical converged solutions, this residue is $10^{-3}$–$10^{-4}$. Convergence is accelerated by as much as a factor of two or three by using two or three grids of successively finer mesh size. The solution is converged in the coarsest grid, which then is subdivided by a factor of two or three in each direction. Starting with coarse-grid solution, a fine-grid solution then can be converged relatively rapidly. This process then may be repeated.

## III. Proofing of Code

The code was proof tested with the following benchmark test cases for which exact theoretical solutions or experimental data were available for comparison.

One-dimensional cases:

1) Riemann's shock tube problem with initial pressure ratios of $10^2$, $10^3$, and $10^4$; EOS 1.

2) Impacts of two zones of ideal gas or dense media (Fe) at closing velocities up to 220 km/s; EOS 1 and 3.

3) Impacts between a moving dense media zone and a fixed dense media zone backed up by an infinitely stiff wall; this geometry allowed initial shocks, reflected shocks, and expansion waves from a free surface to be studied. The material pairs studied were W/W, solid $H_2$/solid $H_2$, and W/solid $H_2$. The first material of each pair is the moving material. Impact velocities up to 100 km/s were studied; EOS 5.

4) A free propagating detonation in a $2H_2 + O_2$ gas mixture; EOS 2.

Two-dimensional cases:

5) Gas flow over a 24 deg half-angle wedge at a Mach number $M$ of 5.5; EOS 1.

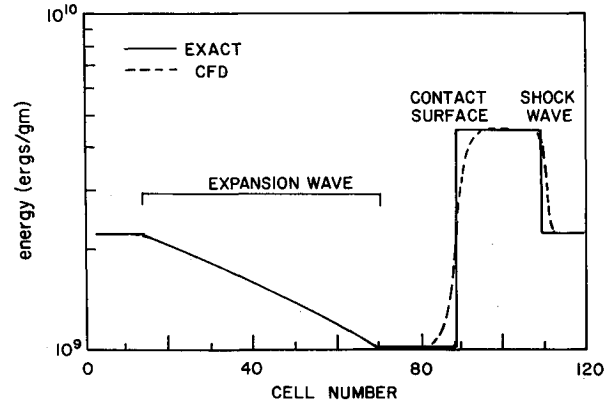


**Fig. 2 Energy profiles for Riemann's shock tube problem for a pressure ratio $R_p$ of 100.**

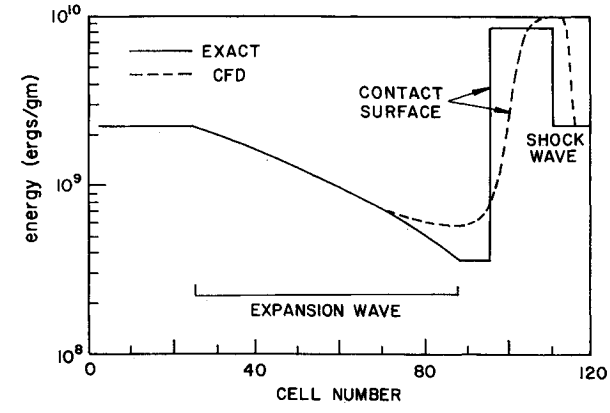


**Fig. 3 Energy profiles for Riemann's shock tube problem for $R_p = 10^4$.**

6) Gas flow over a 30 deg half-angle cone at $M = 3.0$; EOS 1.

7) Dense media (Fe) flow over a 14 deg half-angle wedge at a velocity of 110 km/s; EOS 3.

The EOS numbers refer to the EOS's listed in Sec. II.E. The two-dimensional wedge flow cases had an infinitely stiff wall parallel to the original flow direction so that both an initial and reflected shock were modeled. The SWL procedures (Secs. II.C and II.F) were used only in cases 2, 3, and 7 above (the extremely high-velocity cases).

The code modeling of the benchmark test cases listed above was very good. A few of these cases are discussed below. The most sensitive variable for diagnosing code problems is the internal energy $e$. Figure 2 shows internal energy profiles for Riemann's shock tube problem for a perfect gas with specific heat ratio $\gamma$ of 1.4 and an initial pressure ratio $R_p$ of 100. The diaphragm was located between the 40th and 41st cells. The agreement between the CFD and exact results is excellent. The CFD and exact velocity profiles for this case (not shown) are almost indistinguishable; the only differences are very slight roundings of the CFD solution at the ends of the rarefaction wave and the spreading of the shock wave over a width of about two cells. Figure 3 shows the energy profile comparison for $R_p = 10^4$. Solution degradation is apparent, but acceptable, considering the severity of the test.

Figure 4 and 5 show CFD and exact profiles of $e$ and $p$ for the following test case involving a dense medium—tungsten. (Tabulated SESAME EOS data were used, see Sec. II.E.) A slab of tungsten is initially at rest with an infinitely stiff wall on its right side. An equally thick slab of tungsten, moving toward the right at 100 km/s, impacts the stationary tungsten slab. The interaction produces initial shocks moving outward from the impact plane and, later, a reflected shock from the infinitely stiff wall and a reflected expansion wave from the free surface. Figures 4 and 5 show these latter two waves before they interact. The pressure field is very well predicted by the code. The energy field is reasonably accurately predicted but does show errors of 5–15% in regions where shock waves have developed and in extreme expansion regions. In the latter region, the density is very low (the tungsten has vaporized), and this thus represents an exceedingly severe test for the code. With dense media at very high velocities, the code currently tends to produce energy errors of ~ 10% in a few cells in the regions where strong shock waves develop. This type of energy error was initially ~ 90% when only first-order Godunov calculations were used but was reduced to ~ 10% by using the second-order Godunov calculations as described in Sec. II.D.

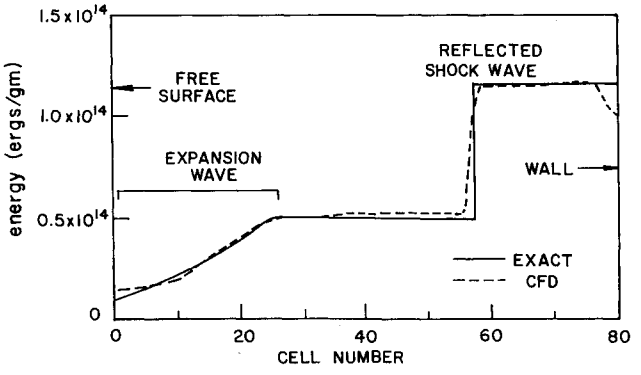


**Fig. 4 Energy profiles for a test case where a slab of tungsten moving from the left at 100 km/s impacts a stationary slab of equal thickness bounded on the right by an infinitely stiff wall. The two initial shocks are reflected as an expansion wave and a shock from the left and right edges of the computational domain, respectively.**

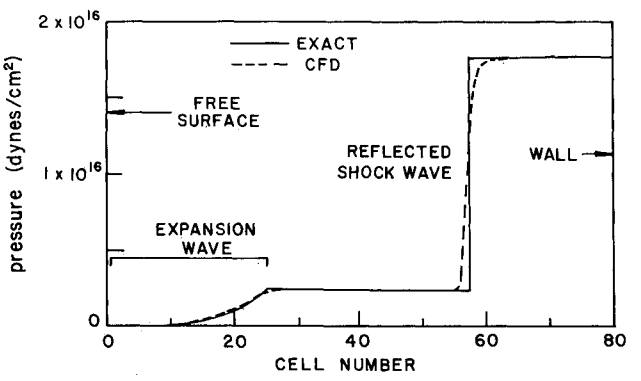


**Fig. 5 Energy profiles for the test case of Fig. 4, except the variable is pressure.**

A calculation was made of a one-dimensional Chapman-Jouguet (C-J) detonation in stoichiometric hydrogen-oxygen initially at 300 K and $10^6$ dynes/cm$^2$ pressure. The detonation is initiated by heating and compressing four cells (of a total of 140) in the center of the computational region. By the last third of the computation, the detonation has reached a nearly constant velocity. Since the code does not, at present, make a true reaction-by-reaction kinetics calculation (see Sec. II.H), the reaction products for the detonation calculations were determined as follows: a number of separate calculations of the equilibrium reactant products at a pressure of $18 \times 10^6$ dynes/cm$^2$ (the C-J detonation pressure) and various temperatures were made. CFD detonation calculations were made for each set of reaction products. The correct set of reaction products was taken to be that one for which the assumed temperature for the equilibrium calculation matched that in the CFD detonation calculation at the thermal choke point—where the reacted flow was moving at Mach 1 away from the detonation front. Table 3 compares predictions for detonation velocity and temperature from the present code with experimental and theoretical results from the literature. The agreement between the results of the present code and results from Refs. 21 and 22 is very good; errors are of the order of 2–3%, at most.

Figure 6 shows a comparison of CFD and exact results for a perfect gas flow (with $\gamma = 1.4$) over a 24 deg half-angle

**Table 3 Comparison of present CFD results and literature data for $2H_2 + O_2$ detonation wave**

| Source | Predicted detonation temperature, K | Predicted detonation velocity, cm/s | Measured detonation velocity, cm/s |
|---|---|---|---|
| Ref. 21 | 3583 | $2.806 \times 10^5$ | $2.819 \times 10^5$ |
| Ref. 22 | 3679 | $2.841 \times 10^5$ | $2.825 \times 10^5$ |
| Present code | 3647 | $2.75 \times 10^5$ | — |
| % error[a] | 0.8–1.8 | 2.0–3.2 | 2.4–2.7 |

[a]This is the present error of the present code results with respect to the literature reference data.

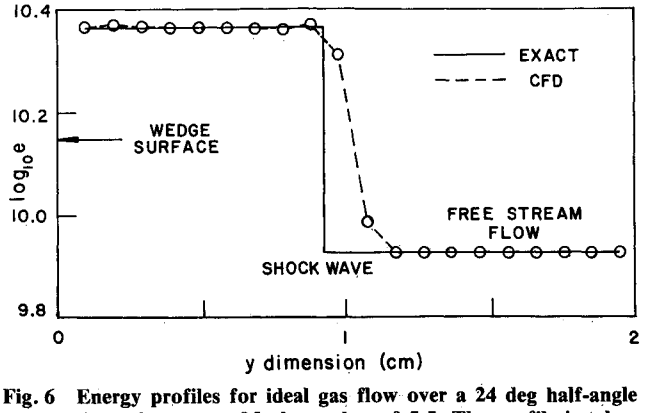


**Fig. 6 Energy profiles for ideal gas flow over a 24 deg half-angle wedge with a freestream Mach number of 5.5. The profile is taken normal to the freestream flow direction ($e$ is in erg/g).**

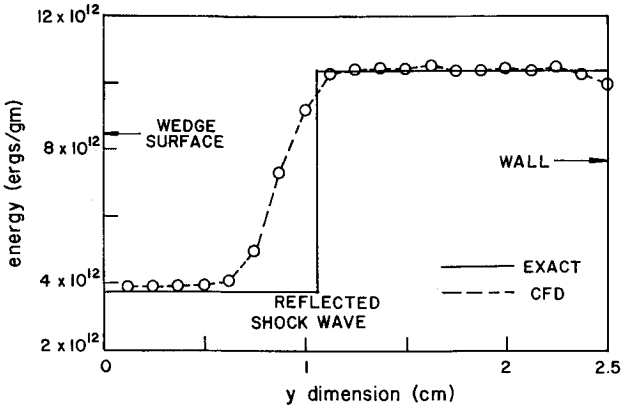


**Fig. 7 Energy profiles for flow of iron over a 14 deg half-angle wedge with a freestream velocity of 110 km/s. There is a wall parallel to the freestream flow direction opposite the wedge. The profile is taken normal to the freestream direction and shows the reflected shock wave.**

wedge. The initial freestream Mach number $M_\infty$ is 5.5. The profiles are of the internal energy $e$ and are taken normal to the initial flow direction, so that, from left to right in the figure, we have the wedge surface, the shock-compressed gas, the shock, and the freestream gas. The errors in the compressed gas $e$ values are less than 2% of the jump in $e$ across the shock. The remaining variables $\rho$, $p$, $u$, and $v$ are predicted with equal or greater accuracy. There is an error of about 1 cell in the shock position.

Figure 7 shows a comparison of CFD and exact results for a flow of iron over a 14 deg wedge. The initial freestream velocity is 110 km/s. The flow is bounded on the side opposite the wedge by a wall parallel to the freestream flow direction so that both initial and reflected shocks are modeled. SESAME EOS data (see Sec. II.E) are used for this calculation. Figure 7 shows profiles of the internal energy taken normal to the freestream direction downstream of the origin of the reflected shock. From left to right in the figure, we see the wedge surface, the medium compressed by the initial shock only, the reflected shock wave, the medium compressed by both shocks and the wall. The modeling of this dense media hypervelocity wedge flow is slightly poorer than that for the gas wedge flow discussed earlier—although very satisfactory, considering the severity of the test. Errors in $e$ (see Fig. 7) and $\rho$ are, at maximum, 3-4% of the shock jumps of $e$ and $\rho$. The corresponding numbers for $p$, $u$, and $v$ are 1-2%. The error in the shock position is essentially zero for the initial shock and about 1.5 cells for the reflected shock.

A comparison also was made of CFD and exact results for flow of a perfect gas (with $\gamma = 1.4$) over a cone with a half-angle of 30 deg. $M_\infty$ was equal to 3.0. The CFD results were found to be in excellent agreement with the exact solution. The errors in $e$, $\rho$, $p$, $u$, and $v$ were, at most, 1-2% of the shock jumps for these variables. The shock was within ½ cell of the correct position.

The overall quality of the CFD solutions obtained in the benchmark test cases is as follows. In most cases, the CFD values of $\rho$ and $e$ are within 2-3% of the exact values, and the CFD values of $p$, $u$, and $v$ are within 1-2% of the exact values. Shocks are crisp, with essentially no oscillations, and with about 80% of the shock jump taking place over a width of two cells. Shocks are usually within 0.5-1.0 cells of their exact position. For wedge flow cases after both the incident and reflected shocks, errors can be slightly larger, reaching 3-4% for $\rho$ and $e$ and 1.0-1.5 cells for the reflected shock position. Some deterioration of solution quality occurs at very high pressure ratios for Riemann's problem (Fig. 3) and in very high velocity impacts of dense media in the regions where shock waves have developed (Fig. 4).

**Table 3 Comparison of present CFD results and literature data for $2H_2 + O_2$ detonation wave**

| Source | Predicted detonation temperature, K | Predicted detonation velocity, cm/s | Measured detonation velocity, cm/s |
|---|---|---|---|
| Ref. 21 | 3583 | $2.806 \times 10^5$ | $2.819 \times 10^5$ |
| Ref. 22 | 3679 | $2.841 \times 10^5$ | $2.825 \times 10^5$ |
| Present code | 3647 | $2.75 \times 10^5$ | — |
| % error[a] | 0.8-1.8 | 2.0-3.2 | 2.4-2.7 |

[a]This is the present error of the present code results with respect to the literature reference data.

Godunov procedures have proved to be much more robust than flux-split procedures in the course of the present studies. Solution of some of the benchmark test cases was attempted by the authors, using MacCormack's[9] correction flux-split procedure and a form of the matrices that diagonalize the flux-state variable Jacobian that are applicable for general EOS's. (The matrices used were similar, but not identical, to those of Ref. 8.) These flux-split procedures were not capable of handling extremely high-velocity impacts (e.g., the cases of Figs. 4 and 5) or the ideal-gas Riemann problem for $R_p$ greater than $\sim 10^3$ (e.g., the case of Fig. 3). In no case were the Godunov procedures inferior to the flux split procedures. The Godunov procedures do not require the assumption that the Euler equations are homogeneous of degree one and do not require the calculation of flux-state variable Jacobians and diagonalizing matrices for explicit methods. The Riemann solver of the Godunov method is readily extendable to second-order accuracy. The present Godunov method is inherently symmetric and for symmetric problems gives symmetric answers down to machine round-off errors. No added smoothing or damping was used, other than that inherent in the extrapolation, interpolation, limiting, and flux calculation procedures. The CPU times for Godunov procedures were found to be essentially the same as those for flux-split procedures.

## IV. Conclusions

An inviscid computational fluid dynamics code has been described that can handle multiple component species, simple chemical reactions, a completely general equation of state, and velocities up to hundreds of kilometers per second. The code uses a sliding grid technique to handle multiple moving zones containing different media. Radiation effects are not treated. Third-order extrapolations and interpolations are used to determine cell boundary values of the primitive variables. Limiting techniques then are applied to these values to maintain code accuracy and stability. First- and second-order Godunov procedures then are used to calculate the cell boundary fluxes. The cell center values then are updated in time using an explicit MacCormack predictor-corrector technique that is second-order accurate in time.

The code was proofed with benchmark test cases including Riemann's shock tube problem at pressure ratios up to $10^4$, impacts of ideal-gas and dense media zones at closing velocities up to 220 km/s, detonation waves in stoichiometric hydrogen-oxygen mixtures, ideal-gas wedge and cone flows, and a wedge flow of iron at a velocity of 110 km/s. The agreement between the CFD results and the exact solutions was excellent.

## Appendix A

See Fig. A1 in reference to the following discussion of interpolation and extrapolation procedures. For interpolation, if the three relevant cell center values of the primitive variables ($x_1$, $x_2$, $x_3$) are well behaved (i.e., do not imply nonmonotonic behavior over the interpolation range), a simple parabolic interpolator is used. If these three values are not well behaved, a first-order "interpolation" $x_2$ is used. Second-order interpolation, i.e., $x_{20}$, is not used because it is equivalent to central differencing and is highly destabilizing. A smooth blend rather

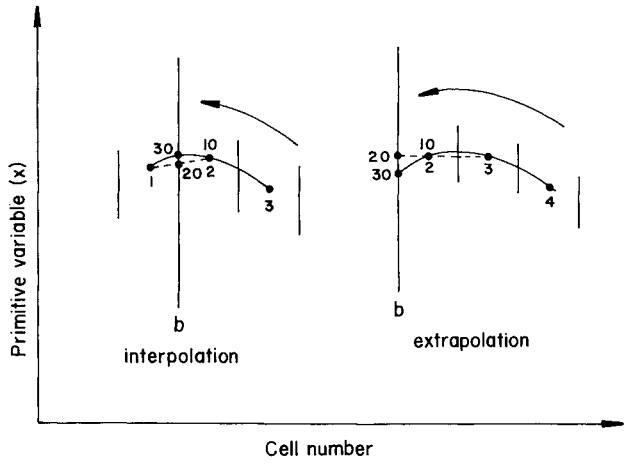


**Fig. A1 Illustrating interpolation and extrapolation procedures (1-4 denote cell center values; 10, 20, 30 denote first-, second-, and third-order interpolations or extrapolations, respectively; *b* is the cell boundary to which the interpolations or extrapolations are made and the curved arrows denote the directions of interpolation or extrapolation).**

than an abrupt switch is made between third- and first-order procedures. The equations used are given below, with $x_b$ being the value of the primitive variable interpolated to the cell boundary $b$:

$$d_{21} = x_2 - x_1 \tag{A1}$$

$$d_{31} = x_3 - x_1 \tag{A2}$$

$$r = d_{21}/d_{31} \tag{A3}$$

$$x_b = x_2,\ r<0 \tag{A4}$$

$$x_b = x_1 + 0.25d_{21},\ 0<r<0.25 \tag{A5}$$

$$x_b = x_1 + 0.75d_{21} - 0.125d_{31},\ 0.25<r<0.75 \tag{A6}$$

$$x_b = x_1 + 2.25d_{21} - 1.25d_{31},\ 0.75<r<1 \tag{A7}$$

$$x_b = x_2,\ 1<r \tag{A8}$$

Equations (A6) is the third-order interpolation, Eqs. (A4) and (A8) the first-order "interpolations," and Eqs. (A5) and (A7) the blends.

A very similar procedure is used for extrapolations, except that when the three relevant cell center values of the primitive values are not well behaved, second-order extrapolations can be used, since they are quite stable. Parabolic third-order extrapolations are used when the relevant cell center values are well behaved. The equations are

$$d_{32} = x_3 - x_2 \tag{A9}$$

$$d_{42} = x_4 - x_2 \tag{A10}$$

$$r = d_{32}/d_{42} \tag{A11}$$

$$x_b = x_2 - 0.5d_{32},\ r<0 \tag{A12}$$

$$x_b = x_2 - 0.125d_{32},\ 0<r<0.3333 \tag{A13}$$

$$x_b = x_2 - 1.25d_{32} + 0.375d_{42},\ 0.3333<r<0.75 \tag{A14}$$

$$x_b = x_2 + 0.25d_{32} - 0.75d_{42},\ 0.75<r<1 \tag{A15}$$

$$x_b = x_2 - 0.5d_{32},\ 1<r \tag{A16}$$

Equations (A12-A16) are third order, lower order, and blend in strict parallel with Eqs. (A4-A8).

## Appendix B

In this Appendix, we outline the second-order Godunov calculation techniques. We assume that all primitive variables have been extrapolated/interpolated to the two sides of the boundary in question, following the procedures described in Secs. II.C and II.F. We rotate the coordinate system so that the $x$ direction (and $u$ velocities) are normal to the boundary and the $y$ direction (and $v$ velocities) are parallel to the boundary.

Conditions are known initially in zones 1 and 5. In general, in the Riemann problem, there will be waves 12 and 45, propagating to the left and right, respectively, with respect to the media, and two new zones, 2 and 4. In extreme expansion conditions, there may be a vacuum zone 3 between zones 2 and 4. Waves 12 and 45 can be shock or expansion waves, and a number of different cases can be identified, depending on whether these waves are shocks or expansions, whether $p_1 > p_5$ or not, and whether $u_1 > u_5$ or not. The number of cases can be reduced to five if $p_1 > p_5$. We will consider only these cases here. If $p_1 < p_5$, zones 1 and 5 are reversed, the Godunov calculation made, and the results reversed again.

The five possible types of solutions to the Riemann problem for $p_1 > p_5$ are outlined in Table B1. Solution of the second-order Godunov problem begins by finding which of cases 1-5 is correct for the data set in question and solving for $p_2$ ($=p_4$) and $u_2$ ($=u_4$) to second-order accuracy. We use the following equation for wave 45 if it is a shock:

$$p_4 - p_5 = \rho_5 c_5 (u_4 - u_5) + \zeta \rho_5 (u_4 - u_5)^2 \tag{B1}$$

where $\zeta = r/(r-1)$ and $r$ is the density ratio of the media for very strong shocks. (A similar equation can be written for wave 12 if it is a shock.) Equation (B1) reduces to the proper acoustic equation for weak waves ($|u_4 - u_5| \ll c_5$) and to the correct expression for strong shock waves ($|u_4 - u_5| \gg c_5$).

We illustrate the handling of an isentropic expansion by considering wave 12 to be isentropic. (Similar equations can be written for wave 45 if it is isentropic.) We evaluate

$$J_1 = -\left.\frac{d^2p}{du^2}\right|_{s,1} = \left.\frac{d(\rho c)}{du}\right|_{s,1} \tag{B2}$$

where the subscript $s$ means along the isentrope. With $J_1$ evaluated from Eq. (B2) and taking $I_1 = \rho_1 c_1$, we write the following equation for wave 12:

$$p_2 - p_1 = -I_1(u_2 - u_1) - (J_1/2)(u_2 - u_1)^2 \tag{B3}$$

This equation reduces to the proper acoustic expression for $|u_2 - u_1| \ll c_1$. For stronger waves, it brings into play a two-term Taylor series expansion about point 1. Under some conditions, $J_1$ may have to be corrected from the value of Eq. (B2) to avoid generating a parabolic curve with Eq. (B3), whose minimum cannot descend to the minimum (complete expansion) pressure $p_{10}$. If $J_1 < -I_1^2/[2(p_1 - p_{10})]$, it is necessary to set $J_1 = -I_1^2/[2(p_1 - p_{10})]$ to avoid this problem. The velocity

**Table B1 Five possible types of solutions to the Riemann problem for $p_1 > p_5$**

| Case | Relation between $u_1$ and $u_5$ | Wave type, wave 12 | Wave type, wave 45 | Vacuum zone between zones 2 and 4 |
|---|---|---|---|---|
| 1 | $u_1 > u_5$ | Shock | Shock | No |
| 2 | $u_1 > u_5$ | Expansion | Shock | No |
| 3 | $u_1 < u_5$ | Expansion | Shock | No |
| 4 | $u_1 < u_5$ | Expansion | Expansion | No |
| 5 | $u_1 < u_5$ | Expansion | Expansion | Yes |

at the complete expansion point can be readily obtained from Eq. (B3) as

$$u_{10} = u_1 + \frac{-I_1 + \sqrt{I_1^2 + 2J_1(p_1 - p_{10})}}{J_1} \tag{B4}$$

Similar equations can be written relating $u_{50}$ and $u_5$.

The first part of the second-order Godunov procedure consists of running through the five cases outlined above in succession, using Eq. (B3) for wave 12 if it is an expansion and the analog of Eq. (B1) if it is a shock and Eq. (B1) for wave 45 if it is a shock and the analog of Eq. (B3) if it is an expansion. For each case, a solution for $p_2(=p_4)$ and $u_2(=u_4)$ is attempted. Since the equations are quadratic, if real solutions are found, there will be two of them; the nonphysical solution is eliminated by checking its disposition with respect to $u_1$, $u_{10}$, $u_5$, and $u_{50}$. If the Godunov procedure is properly set up, there will be only one case (of the five cases described above) with one valid physical solution. With this solution found, the values of $p_2(=p_4)$ and $u_2(=u_4)$ are now known. In the special case of case 5, the two expansion waves are calculated out to their limiting pressures (zero or the media spall strength) and velocities, $p_{10}$, $p_{50}$, $u_{10}$, and $u_{50}$, respectively. Then, $p_2 = p_{10}$, $p_4 = p_{50}$, $u_2 = u_{10}$, $u_4 = u_{50}$, and $u_2 \neq u_4$.

If wave 45 is a shock, the shock wave equations are used to obtain $\rho_4$, $e_4$, and $u_{45}$ (the wave speed) as follows:

$$\rho_4 = \rho_5 \frac{\{1 + \zeta[(u_4 - u_5)/c_5]\}}{\{1 + (\zeta - 1)[(u_4 - u_5)/c_5]\}} \tag{B5}$$

$$e_4 = e_5 + \frac{1}{2}\left(\frac{1}{\rho_5} - \frac{1}{\rho_4}\right)(p_4 + p_5) \tag{B6}$$

$$u_{45} = (\rho_5 u_5 - \rho_4 u_4)/(\rho_5 - \rho_4) \tag{B7}$$

Similar equations may be used to find $\rho_2$, $e_2$, and $u_{12}$ if wave 12 is a shock.

If wave 12 is an expansion wave, second-order integrations are used to find $\rho_2$ and $e_2$. Equation (B3) can be written for a general pressure and velocity along the isentrope, as

$$p - p_1 = -I_1(u - u_1) - (J_1/2)(u - u_1)^2 \tag{B8}$$

Differentials can be taken, yielding

$$dp = -I_1\, du - J_1(u - u_1)\, du \tag{B9}$$

By combining Eqs. (B8) and (B9) with the following differential equations along the isentrope,

$$dp = c^2\, d\rho \tag{B10}$$

$$dp = \rho c\, du \tag{B11}$$

and integrating, one may obtain

$$\frac{1}{\rho_2} = \frac{1}{\rho_1} + \frac{1}{J_1}\ell n\left[1 + \frac{J_1}{I_1}(u_2 - u_1)\right] \tag{B12}$$

a second-order accurate expression for $\rho_2$. By writing Eq. (B12) for general $\rho$ and $u$ along the isentrope and taking differentials, a differential $\rho - u$ equation can be obtained. By combining this equation with Eq. (B8), the differential energy equation along the isentrope,

$$de = \frac{p}{\rho^2}\, d\rho \tag{B13}$$

and integrating, the following second-order accurate expression for $e_2$ can be obtained:

$$e_2 = e_1 + \frac{1}{J_1}\left\{-\left(p_1 + \frac{I_1^2}{2J_1}\right)\ell n\left[1 + \frac{J_1}{I_1}(u_2 - u_1)\right] + \frac{1}{4}(u_2 - u_1)I_1\left[2 + \frac{J_1}{I_1}(u_2 - u_1)\right]\right\} \tag{B14}$$

Equations (B12) and (B14) are second order and are more accurate than the corresponding first-order expressions. However, they are not exact and under severe expansion conditions can predict $\rho_2$ and $e_2$ values less than zero. To avoid code failure stemming from negative densities and internal energies, the following limiting procedure is applied. If $\rho_2 < C_1\rho_1$, $\rho_2$ is set to $C_1\rho_1$, where $C_1$ is a constant. Likewise, if $e_2 < C_1 e_1$, $e_2$ is set to $C_1 e_1$. Most of our results have been obtained with $C_1 = 0.01$. Equations similar to (B12) and (B14) can be obtained for $\rho_4$ and $e_4$ if wave 45 is an expansion. If wave 12 and/or wave 45 are expansions, the wave speeds are taken to be $u_{12} = [(u_1 - c_1) + (u_2 - c_2)]/2$ and $u_{45} = [(u_4 + c_4) + (u_5 + c_5)]/2$, respectively.

From the velocities of the waves, the zone in which the cell boundary will reside during the current step can be found. No attempt is made to locate cell boundaries within an expansion wave; it is either to the left or right of the complete expansion wave system. For case 5, there are two particle path lines, 23 and 34, emanating from the origin in $x - t$ space, instead of the single line 24, which would be the contact surface. These two lines represent the media-vacuum interfaces. The velocity $u_{23}$ is equal to the particle velocity $u_{10}$ of the complete expansion from state 1, and the velocity $u_{34}$ is equal to the particle velocity $u_{50}$ of the complete expansion from state 5. In this case, $u_{23}$ is not equal to $u_{34}$. The primitive variables in the vacuum region are all zero, except for $p$, if the limiting pressure is the spall strength. This is necessary for consistency, since the code does not allow for spall and the sudden appearance of new free surfaces within the solution.

With the zone in which the cell boundary will reside during the current time step known, the fluxes are calculated from the primitive variables in that zone. The transverse velocity $v$ and the mass fractions $m_i$ are handled exactly as in the first-order Godunov technique.

## Acknowledgments

The authors would like to acknowledge a number of very informative conversations with R. W. MacCormack and D. S. Eberhardt during the course of this work.

The work was supported, in part, by U.S. Air Force Contract F08635-84-K0143 and, in part, by U.S. Department of Energy Contract DE-FG06-85ER13382.

## References

[1]Bruckner, A. P., Bogdanoff, D. W., Knowlen, C., and Hertzberg, A., "Investigations of Gasdynamic Phenomena Associated with the Ram Accelerator Concept," AIAA Paper 87-1327, June 1987.

[2]Knowlen, C., Bogdanoff, D. W., Bruckner, A. P., and Hertzberg, A., "Performance Capabilities of the Ram Accelerator," AIAA Paper 87-2152, June 1987.

[3]Hertzberg, A., Bruckner, A. P., and Bogdanoff, D. W., "A New Method for Accelerating Projectiles to Ultrahigh Velocities," *AIAA Journal*, Vol. 26, Feb. 1988, pp. 195–203.

[4]Hertzberg, A., Bruckner, A. P., Mattick, A. T., and Bogdanoff, D. W., "A Chemical Method for Achieving Acceleration of Macroparticles to Ultrahigh Velocities," Aerospace and Energetics Research Program, Univ. of Washington, Seattle, WA, Progress Rept. 1, DOE Grant FG06 85ER13386, June 1, 1985–Feb. 28, 1986.

[5]Fowles, G. R., Leung, C., Rabie, R., and Shaner, J., "Acceleration of Flat Plates by Multiple Staging," *High Pressure Science and Technology*, Vol. 2, edited by K. D. Timmerhaus and M. S. Barber, Plenum, New York, 1977, pp. 911–919.

[6]Warming, R. F. and Beam, R. M., "On the Construction and Application of Implicit Factored Schemes for Conservation Laws," *SIAM-AMS Proceedings*, Vol. 11, Society of Industrial and Applied Mathematics, Philadelphia, PA, 1978, pp. 85–129.

[7]Anderson, D. A., Tannehill, J. C., and Pletcher, R. H., *Computational Fluid Mechanics and Heat Transfer,* McGraw-Hill, New York, 1984, pp. 272–288.

[8]Eberhardt, S. and Palmer, G., "A Two-Dimensional, TVD Numerical Scheme for Inviscid, High Mach Number Flows in Chemical Equilibrium," AIAA Paper 86-1284, June 1986.

[9]MacCormack, R. W., "Current Status of Numerical Solutions of the Navier-Stokes Equations," AIAA Paper 85-0032, Jan. 1985, p. 6.

[10]Eidelman, S., Colella, P., and Shreeve, R. P., "Applications of the Godunov Method and Its Second-Order Extension to Cascade Flow Modeling," *AIAA Journal,* Vol. 22, Nov. 1984, pp. 1609–1615.

[11]Addessio, F. L., Carroll, D. E., Dukowicz, J. K., Harlow, F. H., Johnson, J. N., Kashiwa, B. A., Maltrud, M. E., and Ruppel, H. M., "CAVEAT: A Computer Code for Fluid Dynamics Problems with Large Distortion and Internal Slip," Los Alamos National Lab., Los Alamos, NM, Rept. LA-10613-MS UC-32, Feb. 1986, pp. 119–137.

[12]Yee, H. C., "Upwind and Symmetric Shock-Capturing Schemes," NASA TM 89464, May 1987, pp. 33–34.

[13]Stull, D. R. and Prophet, M. (project directors), *JANAF Thermochemical Tables,* U. S. Government Printing Office, Washington, DC, June 1971.

[14]Zel'dovich, Y. B. and Raizer, Y. P., *Physics of Shock Waves and High-Temperature Hydrodynamic Phenomena,* Vol. II, Academic, New York, 1967, pp. 704–705.

[15]Zel'dovich, Y. B. and Raizer, Y. P., *Physics of Shock Waves and High-Temperature Hydrodynamic Phenomena,* Vol. II, Academic, New York, 1967, pp. 710.

[16]Cooper, N. G. (ed.), "An Invitation to Participate in the LASL Equation of State Library," Los Alamos Scientific Lab., Los Alamos, NM, Rept. LASL-79-62, 1979.

[17]Rudy, D. H. and Strikwerda, J. C., "A Nonreflecting Boundary Condition for Subsonic Navier-Stokes Calculations," *Journal of Computational Physics,* Vol. 36, No. 1, June 1980, pp. 55–70.

[18]MacCormack, R. W., "Current Status of Numerical Solutions of the Navier-Stokes Equations," AIAA Paper 85-0032, June 1985, p. 4.

[19]Anderson, D. A., Tannehill, J. C., and Pletcher, R. H., *Computational Fluid Mechanics and Heat Transfer,* McGraw-Hill, New York, 1984, p. 482–484.

[20]Voevodsky, V. V. and Soloukhin, R. J., "On the Mechanism and Explosion Limits of Hydrogen-Oxygen Chain Self-Ignition in Shock Waves," *Tenth Symposium (International) on Combustion,* The Combustion Institute, Pittsburgh, PA, Aug. 1964, pp. 279–283.

[21]Lewis, B. and von Elbe, G., *Combustion, Flames and Explosions of Gases,* Academic, New York, 1961, p. 527.

[22]Strehlow, R. A., *Combustion Fundamentals,* McGraw-Hill, New York, 1984, p. 304.